Materials Horizons

COMMUNICATION

View Article Online
View Journal | View Issue

Cite this: *Mater. Horiz.*, 2017, 4, 694

Received 27th April 2017,
Accepted 7th June 2017

DOI: 10.1039/c7mh00262a

rsc.li/materials-horizons

A multifunctional skin-like sensor based on a 3D printed thermo-responsive hydrogel†

Zhouyue Lei,[a] Quankang Wang[b] and Peiyi Wu *[ac]

An effective and general strategy is developed to prepare a multifunctional and mechanically compliant skin-like sensor by incorporating a 3D printed thermo-responsive hydrogel into a capacitor circuit. The prepared intelligent skin shows a sensitive and stable capacitance–temperature response, and also exhibits very high pressure sensitivity within 1 kPa, allowing it to sense body temperature, gentle finger touches and finger bending motion. This work not only demonstrates that stimuli-responsive hydrogels are promising candidates for artificially intelligent skins, but might also enrich the design of skin-like sensors for future artificial intelligence, wearable devices and human/machine interaction applications.

Introduction

Inspired by the wide-range of sensory capabilities and mechanical adaptability of human skin, a variety of soft electronics have been developed to imitate skin's unique characteristics in the past few decades.[1] Such devices, also called "artificial skin", can transduce external stimuli such as temperature,[2–4] pressure,[5,6] strain,[6–8] vibration[9] and traces of biomolecules[10] into reliable electronic signals, and thus have provided new opportunities for personal healthcare, wearable devices and soft robotic applications.[11–18] In these rapidly growing fields, significant achievements have been shown in the developments of "electronic skins", which report signals through electrical conductors.[1,19–21] They meet the essential requirements of conductivity and sensory capabilities, but usually struggle to meet additional requirements in terms of low moduli, mechanical adaptability and transparency for a better experience of wearing.[1,20–23]

Conceptual insights

With growing interest in the fields of wearable devices, artificial intelligence and soft robotics, it is challenging and essential to prepare soft sensors that can imitate both the sensory capabilities and mechanical properties of human skin. Generally, ionic sensors based on biocompatible and ionically conductive hydrogels, match well with the mechanical properties of human skin, but their sensory capabilities are limited, *i.e.*, so far only strain and stress sensations have been reported in hydrogel-based ionic sensors. Here, we develop an effective and general strategy to fabricate a multifunctional ionic skin by incorporating a printable and thermo-responsive hydrogel with grid microstructures into a capacitor circuit. In the circuit, the hydrogel has a low modulus and thus ensures mechanical compliance, and 3D printed microstructures can magnify capacitive area variations upon external stimuli such as temperature and pressure, which allows the hydrogel-based devices to sense body temperature and human motion. This study not only presents a simple and promising strategy to transduce the volume phase transition behaviours of stimuli-responsive hydrogels into reliable electrical signals, but might also be helpful to develop biocompatible hydrogel-based sensors with a wide range of sensory capabilities for future soft robotics and human/machine interaction applications.

To address these challenges, the development of novel materials is critical. Recently, on the basis of the concept of "ionic skin" proposed by Whitesides and Suo,[24] soft, biocompatible and ionically conductive hydrogels, have shown great potential in the field of artificially intelligent skins. Different from electronic skins usually fabricated from organic elastomer matrices embedded with inorganic conductive materials, hydrogel materials have similar physiological and mechanical properties to human skin, which is mainly composed of biomacromolecular networks infiltrated with water. Thus hydrogels can monitor soft tissues without constraining them and usually have better biocompatibility for wearable devices.[24,25] In addition to the ionic skins based on chemically crosslinked polyacrylamide (PAM) hydrogels[24,26–29] or an ionic fluid,[30] our recent work also developed a mechanically adaptable and highly sensitive ionic skin made up of a physically crosslinked hydrogel.[25] This hydrogel is composed of very small amorphous calcium

[a] *State Key Laboratory of Molecular Engineering of Polymers, Department of Macromolecular Science and Laboratory for Advanced Materials, Fudan University, Shanghai 200433, China. E-mail: peiyiwu@fudan.edu.cn*
[b] *Department of Physics, Fudan University, Shanghai 200433, China*
[c] *State Key Laboratory for Modification of Chemical Fibers and Polymer Materials & College of Chemistry, Chemical Engineering and Biotechnology, Center for Advanced Low-Dimension Materials, Donghua University, Shanghai 201620, China*

† Electronic supplementary information (ESI) available: Rheological analyses, theoretical simulations, Fig. S1–S10 and Movies S1. See DOI: 10.1039/c7mh00262a

carbonate (ACC) nanoparticles physically crosslinked by polyacrylic acid (PAA) and alginate chains, and reports signals using free Ca^{2+} dissolved from ACC. Due to its dynamically physical crosslinking effect, the hydrogel and corresponding ionic skin are autonomously self-healable and mechanically compliant to curved and dynamic surfaces, and exhibit relatively high pressure sensitivity. However, compared with various sensations demonstrated in electronic skins, the sensory capabilities of ionic skins are still limited. For instance, sensing temperature has not yet been achieved, although it is a key functionality of human skin that provides information about the surrounding natural environment. Fortunately, inspired by numerous reports on stimuli-responsive hydrogels, whose volume phase transition behaviors and mechanical properties can be tailored by designing different microscopic interpenetrating polymer networks or incorporating sensitive moieties in hydrogels,[31–34] we believe that widely reported stimuli-responsive hydrogels are promising candidates to be applied as novel skin-inspired ionic sensors. However, there still remained two problems: (1) how to transduce the volume phase transition behaviors into reliable electronic signals and (2) how to enhance the responsive amplitude of stimuli-responsive hydrogels, which determines the sensitivity of the sensors and depends on the size of the sample and the collective diffusion of the polymer network.[35]

Herein, we propose a feasible strategy that incorporates stimuli-responsive microstructured hydrogels into a capacitor circuit. This design is based on two key points: (1) capacitive sensors in a parallel-plate configuration are sensitive to changes in conductive area,[24] and thus allow area changes in the stimuli-responsive conductors to be transduced into capacitance signals; (2) microstructuring the conductive layers with a sub-millimeter resolution could enhance the relative area changes upon stimulation, and thereby magnify the capacitive response signals. As a proof-of-concept study, a 3D printed thermo-responsive hydrogel with double networks was designed for fabricating a thermal skin-like sensor. It underwent phase transition when the temperature increased, resulting in the disentanglement of the physical crosslinks and thus decreased the viscosity for 3D printing to fabricate microstructures. The expanding area at high temperature also allowed for capacitance-temperature responses; in particular, a grid structure magnified the geometric area changes. Benefitting from this rational design, the resulting skin-like hydrogel sensor exhibited high sensitivity upon thermal or pressure stimuli. Such characteristics not only pave the way for a feasible approach to realize electrical signal transduction on stimuli-responsive hydrogels, but might also promote the development of skin-inspired ionic devices with a wide range of sensory capabilities.

Results and discussion

A printable and thermo-responsive double-network hydrogel was synthesized by using a micellar-copolymerization method. During the polymerization process, hydrophobic *n*-octadecyl acrylate (C18) domains were stabilized by sodium dodecylsulfate (SDS) micelles, whose crystallizable side chains acted as reversible physical crosslinks,[36] and meanwhile, a loose covalent network was also formed probably due to the chain transfer reaction in *N*,*N*-dimethylacrylamide (DMA) polymerization (Fig. S1, ESI†).[37] As a result, the micellar-copolymerization process yields composite networks composed of physically crosslinked crystalline domains imbedded in the covalent network. The hydrogel (DMA:C18 = 1 : 1) displayed a compressive modulus of 11 kPa (Fig. S2, ESI†) at 20 °C, which was close to the Young's modulus of the human body and thus ensured mechanical compatibility between the hydrogel devices and human tissue.[38] According to the rheological characterization in Fig. S3 (ESI†), it exhibited elastically solid-like behavior at room temperature (the storage modulus $G' >$ the loss modulus G''), while the moduli decreased at increasing temperature. A turning-point around 30 °C indicated the volume phase transition temperature (VPTT), which was consistent with the phase transition temperature determined by turbidity (Fig. S4, ESI†) and differential scanning calorimetry (DSC) measurements (Fig. S5, ESI†). The small differences are probably due to different measurement mechanisms. When varying the molar ratio of DMA and C18, the phase transition temperatures were slightly different, suggesting that the VPTT of this double-network hydrogel was relatively stable. This phase transition behavior can also be traced by temperature-variable infrared (IR) spectra. As shown in Fig. S6 (ESI†), upon heating, the C═O stretching band shifted to higher wavenumbers, which should represent the C18 chain disordering and the disentanglement of the physically crosslinked network during melting. Overall, the VPTT arises from the crystallizable moieties in the hydrogels and locates at around 30 °C, close to human body temperature.

Upon heating the hydrogels above the VPTT, the disentanglement of the physically crosslinked network results in a lowered viscosity with a shear-thinning characteristic, which is suitable for 3D printing to re-construct hydrogel architectures. Fig. 1a depicts the viscosity and stress as a function of shear rates. At a low shear rate (1 s^{-1}), the viscosity was 365 Pa s, while at a high shear rate (500 s^{-1}), the viscosity decreased to about 1 Pa s, which was desirable for extrusion. This shear-thinning behavior could be quantitatively analysed by a power-law fluid model. The shear-thinning exponent n was calculated to be 0.14 in the high-strain rate region (1–500 s^{-1}). When the power-law fluid flows through a cylindrical tube of radius r, the shear rate $\dot{\gamma}$ can be predicted by the Rabinowitsch–Mooney equation.[39] Since the suitable viscosity for 3D extrusion printing should be in the range of 0.1–10 Pa s,[39,40] the tip diameter of 0.41 mm and an extrusion speed of 6 mm s^{-1} were chosen in this work. The corresponding viscosity was calculated to be about 1.5 Pa s. After extrusion, the recovery of a higher viscosity allowed for shape retention. The calculation details can be seen in the ESI.† Printing was performed using an extrusion 3D printing workstation equipped with an ink extrusion system, a precise positioning system and a hardware/software interface to control the extrusion rates and locations of the samples (Fig. 1b and c and Movie S1, ESI†).

The printed grid-structured hydrogel film was flexible and had a sub-millimeter resolution (Fig. 1d and e). The rheological

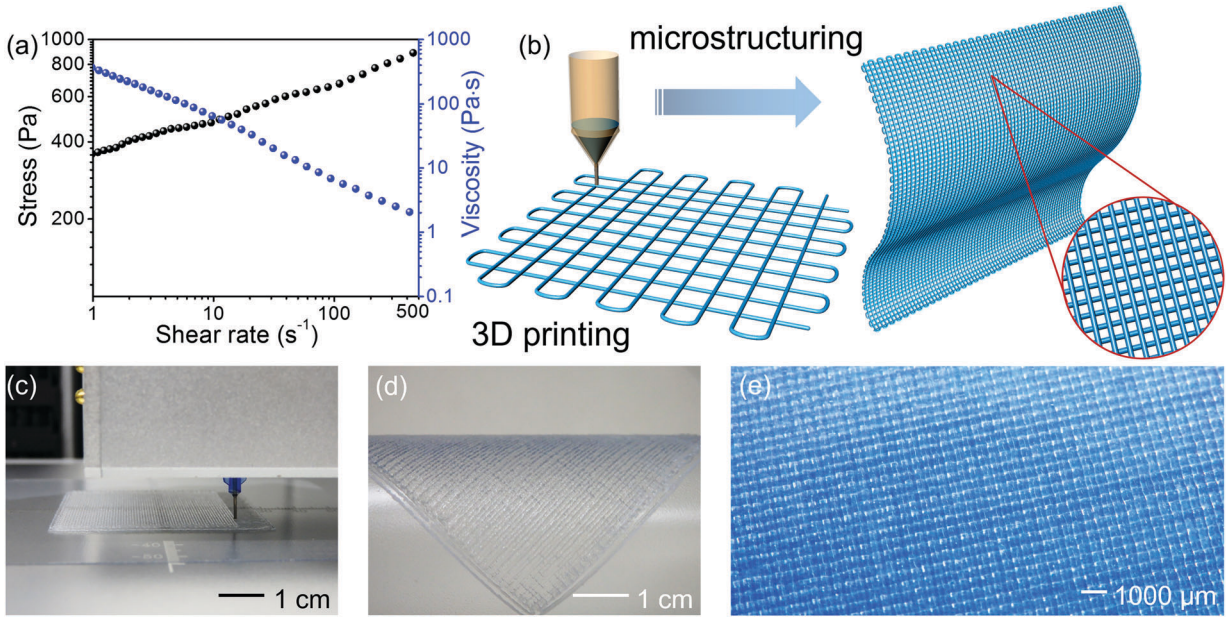

Fig. 1 (a) Viscometry results of the thermo-responsive hydrogel (stress and viscosity against different shear rates). (b) Schematic illustration of the 3D printing process and the grid microstructure of a printed hydrogel film. (c) A photo of the 3D printing process. (d) A photo of the printed flexible hydrogel film. (e) A photo of the grid-structured hydrogel with a sub-millimeter resolution.

behavior (Fig. S7, ESI†) of the grid-structured hydrogel film was also characterized, similar to the bulk hydrogel.

In the presence of salt solutes, the hydrogel is ionically conductive and thus enables the fabrication of capacitance devices.[24,29] Here, we constructed a skin-like capacitive sensor by integrating two grid-structured hydrogel films with a dielectric polyethylene layer, as shown in Fig. 2. The capacitance C measured between two electrodes is dominated by the capacitance of the dielectric C_D,[24] as shown in Fig. 2b. Based on the relationship of the deformation and capacitance in a parallel-plate configuration, $C = \varepsilon S/4\pi kd$ (C is the capacitance, S is the effective area of the ionically conductive layer, d is the thickness of the dielectric polyethylene layer, ε is the dielectric constant of the dielectric layer and k is the electrostatic constant), the capacitive response can be tuned by the geometric area changes. Specifically, when the bulk hydrogel is microstructured with a sub-millimeter resolution, it magnifies the effective area variation and thus results in more sensitively capacitive response upon external stimuli. As shown in Fig. S8 (ESI†), compared with the bulk hydrogel, the printed grid-structured hydrogel with a sub-millimeter resolution showed an enhanced capacitive response when the temperature increases.

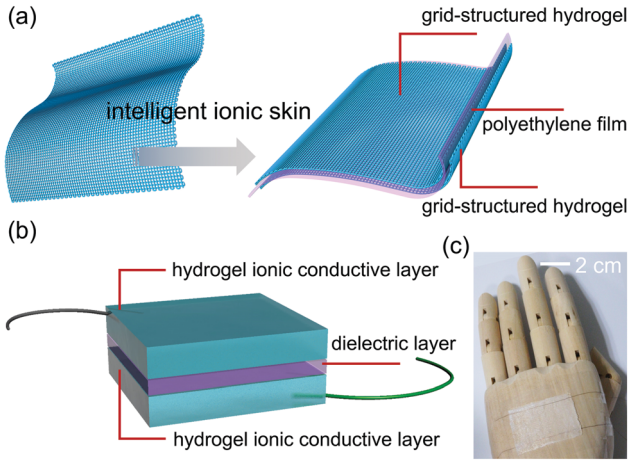

Fig. 2 (a) Schematic illustration of an ionic skin fabricated from the printed hydrogel films. (b) Schematic design of a capacitive sensor device. (c) A photo of the prepared thermo-responsive ionic skin that was attached to a prosthetic hand at room temperature.

Fig. 3a illustrates the predictable capacitive response as a function of grid (fiber) diameter. Due to the parallel-plate configuration in this work, capacitive area changes linearly depend on the changes of the diameters in contact with the dielectric layer. To estimate the relationship of the contacting diameters and the observed diameters, the cross section of a printed hydrogel fiber could be considered as an ellipse in a simplified model, in which the major axis width ($2a$) is the observed fiber diameter and the contacting diameter ($2|x_c|$) could be expressed in an orthogonal coordinate. On the basis of the mathematical calculations in the ESI,† the contacting diameters almost linearly depend on the widths of the major axis. Consequently, the capacitance values are also linearly related to the observed fiber diameters in theory. Here we recorded optical microscopy images of the hydrogel fibers and measured capacitance changes in the grid-structured hydrogel sensors at different temperatures, and then illustrated the actual diameter–capacitance–temperature relationships (Fig. 3b–d). It is worthwhile to note that the hydrogel became transparent when the temperature was above 26 °C, in line with the turbidity result in Fig. S4 (ESI†), and gradually expanded at higher temperature, which was consistent with the capacitance changes. Around VPTT, it indeed displayed a linear relationship between the capacitance

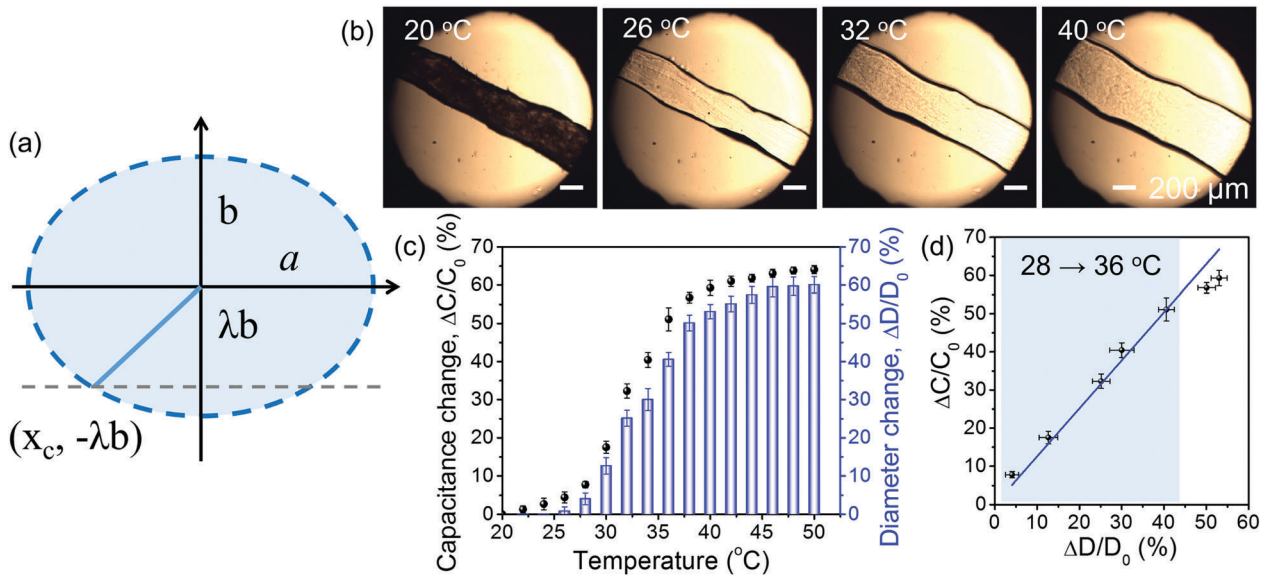

Fig. 3 (a) A simplified mathematical model that was applied to predict effective capacitive area (contacting diameter) changes during heating. (b) Typical optical microscopy images of a printed hydrogel fiber at different temperatures. (c) The capacitance–temperature and diameter–temperature relationships of the thermo-responsive ionic skin in the temperature range of 20–50 °C. (d) The relationship between the capacitance and the diameter changes in the thermo-responsive ionic skin.

and the diameter variations (Fig. 3d), matching well with the theoretical prediction. Furthermore, in order to realize a predictable capacitance-temperature response in a broader temperature range, it is important to regulate the volume phase transition behaviours of common thermo-responsive hydrogels and develop hydrogels with linearly thermo-responsive behaviours.[41]

Since the VPTT of this hydrogel is close to body temperature, the grid-structured hydrogel could be applied as a wearable thermal sensor. Two photographs of the thermal sensor are shown in Fig. 4a and b. It is notable that the hydrogel sensor was opaque when attached to a prosthetic hand (5 °C), while it became transparent on a human hand, due to the phase transition around 30 °C. Meanwhile, the capacitance was increased due to the expanding ionically conductive area. As shown in Fig. 4c, the prepared sensor was transferred between the prosthetic hand and the human hand for ten cycles. Although the baseline drifted in this dynamic temperature sensing process, the relative capacitance changes retained around 37% for ten cycles, indicating a stable thermal response.

The grid microstructure of the skin-like hydrogel sensor also improves its pressure sensitivity. As shown in Fig. 5a, the capacitance was almost linearly responsive to the compressive pressure within 1 kPa. The pressure sensitivity S was calculated from the slope of the trace.[5] As expected, the bulk hydrogel showed a relatively low sensitivity (0.09 kPa^{-1}). Notably, the pressure sensitivity of the grid-structured hydrogel was up to 0.45 kPa^{-1}, with an order of magnitude increase. Compared to previously reported skin-like pressure sensors (Fig. S9, ESI†), the microstructured hydrogel is comparable to microstructured PDMS films,[5] and shows a better performance than those unstructured ones based on physically crosslinked mineral hydrogels,[25] chemically crosslinked polyacrylamide (PAAm),[24] bulk poly (dimethylsiloxane) (PDMS),[5] *etc.*

To demonstrate potential applications of the microstructured hydrogel as a human motion sensor, it was attached to a prosthetic hand or a human finger. Notably, the microstructured hydrogel displayed increased capacitance changes compared with the

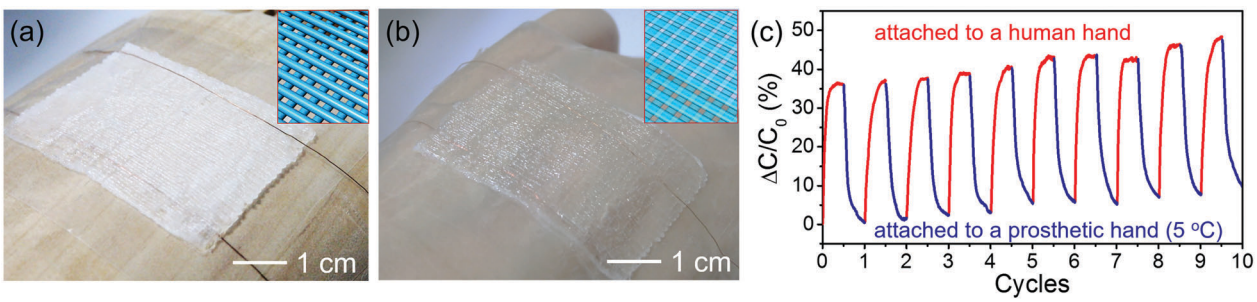

Fig. 4 (a) A photo of the prepared thermo-responsive ionic skin that was attached to a prosthetic finger at 5 °C. (b) A photo of the prepared thermo-responsive ionic skin that was attached to a human hand. The insets schematically illustrate the different grid structures at different temperatures. (c) The stable capacitive response of the thermo-responsive ionic skin when it was dynamically transferred between a prosthetic hand (5 °C) and a human hand.

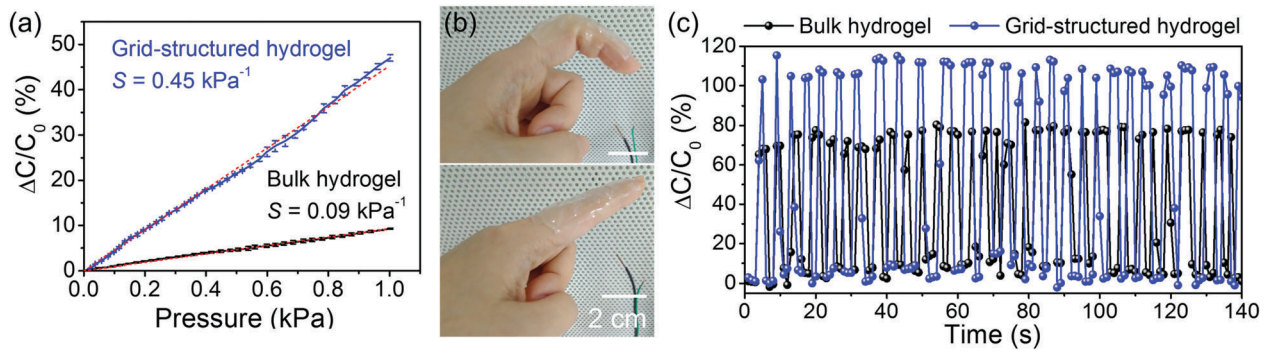

Fig. 5 (a) The capacitance–pressure curves of a bulk hydrogel sensor and a grid-structured hydrogel sensor in the range of 0–1 kPa. (b) Photos of the grid-structured hydrogel sensor attached to a bent/straight finger. (c) Capacitance signals of the bulk hydrogel sensor and the grid-structured hydrogel sensor as the finger bend cyclically.

bulk one. As shown in Fig. S10 (ESI†) and Fig. 5b and c, the grid-structured hydrogel could sense gentle finger touches (<1 kPa), and conformably contacted with the human body to monitor finger bending motion. The capacitance increased rapidly upon bending the finger and could fully recover upon unbending. These examples show the great potential of this grid-structured hydrogel for future human/machine interaction and human motion monitoring applications.

We further examined the capacitive response upon a mutual effect of pressure and temperature stimuli. The understanding of how both stimuli affect the hydrogel-based intelligent skin was established by exposing it to a range of pressures at different temperatures. As shown in Fig. 6, in the temperature range from room temperature (20 °C) to body temperature (36 °C), the hydrogel sensor's capacitance–pressure response (0–0.9 kPa) exhibits an approximately linear relationship. While the sensor's temperature dependence shows an abrupt change around 28 °C. Before VPTT, the temperature has no significant influence on the capacitance, but it shows about 5% capacitance change when the temperature rises by 1 °C in the range of 28–36 °C. This capacitance–temperature trend is similar at different pressures (0–0.9 kPa). The hydrogel sensor's capacitive response on pressure (P) and temperature (T) can be described as a hyperplane in the "capacitance change *vs.* pressure *vs.* temperature" space (Fig. 6), which achieves roughly multi-parametric sensing. However, this hydrogel sensor did not exhibit a linear response towards pressure and temperature in a wide range, compared to previously reported electronic skins.[42] More accurate prediction could be realized by further regulating the sensor's structure and using better algorithms.[43–46]

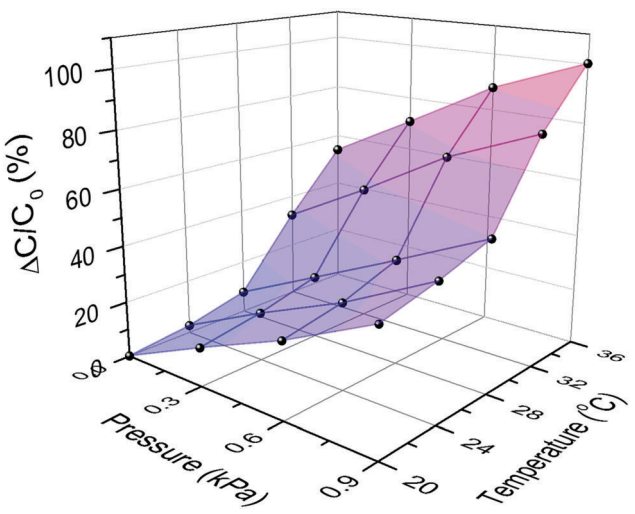

Fig. 6 The capacitive response of the hydrogel sensor upon applying pressure and temperature. Each point plotted was derived from averaging the values derived from at least 3 collected data points, as measured under the same conditions.

Conclusions

In summary, we present a multifunctional skin-like sensor based on a thermo-responsive double-network hydrogel. In the presence of a reversible physically crosslinked network, the hydrogel's rheological behavior is tunable and suitable for an advanced 3D printing technique to construct microstructures with a sub-millimeter resolution. This capability allows the fabrication of an ionic cable array and thus magnifies the capacitive response signals as a function of the fiber diameter changes. The strategies employed here not only develop the first example of a thermo-responsive, highly sensitive and mechanically compliant ionic skin, but also provide a simple pathway to realize electrical signal transduction on stimuli-responsive hydrogels and might enrich the design of intelligent ionic devices based on hydrogels for future human/machine interactions and soft robotic applications.

Experimental section

Materials

DMA, SDS, NaCl, ammonium persulfate (APS) and sodium metabisulfite (SMS) were purchased from Aladdin Co. Ltd, and C18 was purchased from TCI Co. Ltd. DMA monomer was purified by passing it through an alumina column. Unless otherwise specified, all other reagents were of analytical grade and used without further purification. N_2 with a purity of 99.9% was purchased from Shanghai Jifu Gas Co. Ltd.

Preparation of PDMA-C18 hydrogels

The hydrogels were prepared by micellar copolymerization of DMA and C18 at 55 °C in 4.4 wt% NaCl aqueous solution containing 11 wt% SDS, in which NaCl was added into the surfactant solution to induce micellar growth and thus solubilize hydrophobic C18 in the SDS micelles.[36] The total monomer concentration was 0.5 M and the molar ratio of DMA and C18 was varied from 3 : 1 to 1 : 1. Note that a higher monomer concentration would result in higher viscosities which were not suitable for 3D printing. The polymerization reaction was initiated using a redox initiator system consisting of 0.4 mM APS and 0.5 mM SMS at 55 °C for 24 h. The following preparation and characterization processes are based on the hydrogel with a monomer molar ratio of 1 : 1, unless otherwise stated.

Control experiments for preparing PDMA and PDMA/NaCl/SDS hydrogels

To confirm that a loose covalent network was formed probably due to the chain transfer reaction of DMA monomers, pure PDMA and PDMA/NaCl/SDS hydrogels were also prepared using the same procedure.

3D printing of the PDMA-C18 hydrogel

The prepared hydrogels were printed using a 3D printing system (3D Bio-Architect® work station, Regenovo). The hydrogels were firstly loaded into an extrusion cartridge with a temperature controller. After melting at 45 °C for at least an hour, the homogeneous, low-viscosity and transparent hydrogels were then extruded using a flat tip needle with a diameter of 0.41 mm at an extrusion speed of 6 mm s^{-1}. The temperature of the platform was 10 °C. The hydrogel films were printed for two layers with a rotation angle of 90° and the lateral center-to-center spacing was 0.6 mm. During printing, the hydrogels experienced shear thinning and quickly recovered their viscosity upon exiting.

Device fabrication

A dielectric layer (polyethylene film, 30 μm) was sandwiched between two ionic conductors (bulk/grid-structured hydrogels) which were connected to two metallic electrodes, resulting in a capacitive sensor. For capacitance-compression/temperature tests, an additional two layers of polyethylene films were put on the top and bottom of the sensor to insulate the sensor and prevent water evaporation. When the device was applied as a finger motion sensor, it was fixed between two layers of VHB tape and then attached to a finger.

Characterization

Crystal-melting transition of the hydrogel was observed using an optical microscope (Leica DM2500P, Germany) with a THMS600 hot stage (Linkam, UK). Turbidity measurement was performed at 500 nm on a Lamda 35 UV-vis spectrometer using deionized water as the reference with a heating/cooling rate of 1 °C min^{-1} between 20 and 50 °C. The hydrogel samples for DSC measurements were conducted on a Mettler-Toledo thermal analyzer at a scanning rate of 5 °C min^{-1} from 15 to 50 °C under a nitrogen atmosphere. The hydrogel sample for IR measurements was sandwiched between two ZnS tablets. Temperature-variable IR spectra were collected on a Nicolet Nexus 6700 spectrometer with a resolution of 4 cm^{-1} and 32 scans. Temperatures were controlled using an electronic cell holder at a rate of 1 °C min^{-1} between 20 and 50 °C. All rheological measurements were performed on a HAAKE MARS modular advanced rheometer using the 25 mm parallel-plate geometry. In an oscillation mode with a strain of 1%, a dynamic frequency sweep was conducted from 0.1 to 10 Hz at 20 °C and a dynamic temperature sweep was performed from 20 to 50 °C at 1 Hz. Viscometry was performed at 45 °C with shear rates ranging from 1 to 500 s^{-1}. Compression tests were performed on a tensile machine (CMT4104) at a deformation rate of 1 mm min^{-1} at 20 °C. Capacitance measurements were carried out using an LCR meter (TH2830) at an AC voltage of 1 V and a sweeping frequency of 1 kHz. Capacitance changes were simultaneously detected with various stimuli on the prepared devices. When we examined the capacitive response upon a mutual effect of pressure and temperature stimuli, the sensor was exposed to a range of pressures (applied by glass plates with known weight) at different temperatures. Error bars are the standard deviation of at least 3 collected data points, which are measured under the same conditions.

Acknowledgements

We gratefully acknowledge the financial support from the National Science Foundation of China (No. 21674025 and 51473038) and the Ministry of Science & Technology of China (No. 2016YFA0203302). We also thank Prof. Shengtong Sun of the Donghua University for helpful discussion.

Notes and references

1 A. Chortos, J. Liu and Z. Bao, *Nat. Mater.*, 2016, **15**, 937.
2 J. Jeon, H.-B.-R. Lee and Z. Bao, *Adv. Mater.*, 2013, **25**, 850.
3 R. C. Webb, A. P. Bonifas, A. Behnaz, Y. Zhang, K. J. Yu, H. Cheng, M. Shi, Z. Bian, Z. Liu, Y.-S. Kim, W.-H. Yeo, J. S. Park, J. Song, Y. Li, Y. Huang, A. M. Gorbach and J. A. Rogers, *Nat. Mater.*, 2013, **12**, 938.
4 H. Yang, D. Qi, Z. Liu, B. K. Chandran, T. Wang, J. Yu and X. Chen, *Adv. Mater.*, 2016, **28**, 9175.
5 S. C. B. Mannsfeld, B. C. K. Tee, R. M. Stoltenberg, C. V. H. H. Chen, S. Barman, B. V. O. Muir, A. N. Sokolov, C. Reese and Z. Bao, *Nat. Mater.*, 2010, **9**, 859.
6 J. Mu, C. Hou, G. Wang, X. Wang, Q. Zhang, Y. Li, H. Wang and M. Zhu, *Adv. Mater.*, 2016, **28**, 9491.
7 D. J. Cohen, D. Mitra, K. Peterson and M. M. Maharbiz, *Nano Lett.*, 2012, **12**, 1821.
8 X. Liao, Z. Zhang, Z. Kang, F. Gao, Q. Liao and Y. Zhang, *Mater. Horiz.*, 2017, **4**, 502.
9 Y.-C. Lai, J. Deng, S. Niu, W. Peng, C. Wu, R. Liu, Z. Wen and Z. L. Wang, *Adv. Mater.*, 2016, **28**, 10024.
10 G. Wang, G. Shi, H. Wang, Q. Zhang and Y. Li, *Adv. Funct. Mater.*, 2014, **24**, 1017.

11 A. Chortos and Z. Bao, *Mater. Today*, 2014, **17**, 321.
12 S. Bauer, S. Bauer-Gogonea, I. Graz, M. Kaltenbrunner, C. Keplinger and R. Schwödiauer, *Adv. Mater.*, 2014, **26**, 149.
13 X. Wang, L. Dong, H. Zhang, R. Yu, C. Pan and Z. L. Wang, *Adv. Sci.*, 2015, **2**, 1500169.
14 S. Lim, D. Son, J. Kim, Y. B. Lee, J.-K. Song, S. Choi, D. J. Lee, J. H. Kim, M. Lee, T. Hyeon and D.-H. Kim, *Adv. Funct. Mater.*, 2015, **25**, 375.
15 Y. Zang, F. Zhang, C.-a. Di and D. Zhu, *Mater. Horiz.*, 2015, **2**, 140.
16 T. Q. Trung and N.-E. Lee, *Adv. Mater.*, 2016, **28**, 4338.
17 M. Amjadi, K.-U. Kyung, I. Park and M. Sitti, *Adv. Funct. Mater.*, 2016, **26**, 1678.
18 Y. Guo, K. Li, C. Hou, Y. Li, Q. Zhang and H. Wang, *ACS Appl. Mater. Interfaces*, 2016, **8**, 4676.
19 D.-H. Kim, N. Lu, R. Ma, Y.-S. Kim, R.-H. Kim, S. Wang, J. Wu, S. M. Won, H. Tao, A. Islam, K. J. Yu, T.-i. Kim, R. Chowdhury, M. Ying, L. Xu, M. Li, H.-J. Chung, H. Keum, M. McCormick, P. Liu, Y.-W. Zhang, F. G. Omenetto, Y. Huang, T. Coleman and J. A. Rogers, *Science*, 2011, **333**, 838.
20 M. L. Hammock, A. Chortos, B. C. K. Tee, J. B. H. Tok and Z. Bao, *Adv. Mater.*, 2013, **25**, 5997.
21 T. Someya, Z. Bao and G. G. Malliaras, *Nature*, 2016, **540**, 379.
22 S. J. Benight, C. Wang, J. B. H. Tok and Z. Bao, *Prog. Polym. Sci.*, 2013, **38**, 1961.
23 A. J. Bandodkar, I. Jeerapan and J. Wang, *ACS Sens.*, 2016, **1**, 464.
24 J.-Y. Sun, C. Keplinger, G. M. Whitesides and Z. Suo, *Adv. Mater.*, 2014, **26**, 7608.
25 Z. Lei, Q. Wang, S. Sun, W. Zhu and P. Wu, *Adv. Mater.*, 2017, **29**, 1700321.
26 C. H. Yang, B. Chen, J. Zhou, Y. M. Chen and Z. Suo, *Adv. Mater.*, 2016, **28**, 4480.
27 C. Larson, B. Peele, S. Li, S. Robinson, M. Totaro, L. Beccai, B. Mazzolai and R. Shepherd, *Science*, 2016, **351**, 1071.
28 C.-C. Kim, H.-H. Lee, K. H. Oh and J.-Y. Sun, *Science*, 2016, **353**, 682.
29 C. H. Yang, B. Chen, J. J. Lu, J. H. Yang, J. Zhou, Y. M. Chen and Z. Suo, *Extreme Mech. Lett.*, 2015, **3**, 59.
30 A. Frutiger, J. T. Muth, D. M. Vogt, Y. Mengüç, A. Campo, A. D. Valentine, C. J. Walsh and J. A. Lewis, *Adv. Mater.*, 2015, **27**, 2440.
31 S.-k. Ahn, R. M. Kasi, S.-C. Kim, N. Sharma and Y. Zhou, *Soft Matter*, 2008, **4**, 1151.
32 X. Yan, F. Wang, B. Zheng and F. Huang, *Chem. Soc. Rev.*, 2012, **41**, 6042.
33 Z. Lei, W. Zhu, S. Sun and P. Wu, *Nanoscale*, 2016, **8**, 18800.
34 H. Shigemitsu and I. Hamachi, *Acc. Chem. Res.*, 2017, **50**, 740.
35 T. Gancheva and N. Virgilio, *Macromolecules*, 2016, **49**, 5866.
36 C. Bilici, V. Can, U. Nöchel, M. Behl, A. Lendlein and O. Okay, *Macromolecules*, 2016, **49**, 7442.
37 X. Hu, M. Vatankhah-Varnoosfaderani, J. Zhou, Q. Li and S. S. Sheiko, *Adv. Mater.*, 2015, **27**, 6899.
38 X. Chen, *Small Methods*, 2017, 1600029.
39 K. Tian, J. Bae, S. E. Bakarich, C. Yang, R. D. Gately, G. M. Spinks, M. in het Panhuis, Z. Suo and J. J. Vlassak, *Adv. Mater.*, 2017, **29**, 1604827.
40 F. Zhu, L. Cheng, J. Yin, Z. L. Wu, J. Qian, J. Fu and Q. Zheng, *ACS Appl. Mater. Interfaces*, 2016, **8**, 31304.
41 L. Hou and P. Wu, *Macromolecules*, 2016, **49**, 6095.
42 M. Segev-Bar, A. Landman, M. Nir-Shapira, G. Shuster and H. Haick, *ACS Appl. Mater. Interfaces*, 2013, **5**, 5531.
43 N. T. Tien, S. Jeon, D.-I. Kim, T. Q. Trung, M. Jang, B.-U. Hwang, K.-E. Byun, J. Bae, E. Lee, J. B. H. Tok, Z. Bao, N.-E. Lee and J.-J. Park, *Adv. Mater.*, 2014, **26**, 796.
44 S. Harada, W. Honda, T. Arie, S. Akita and K. Takei, *ACS Nano*, 2014, **8**, 3921.
45 M. Segev-Bar, N. Bachar, Y. Wolf, B. Ukrainsky, L. Sarraf and H. Haick, *Adv. Mater. Technol.*, 2017, **2**, 1600206.
46 H. Jin, Y. S. Abu-Raya and H. Haick, *Adv. Healthcare Mater.*, 2017, 1700024.

